Rock Discrimination in the Complex Geologic Environment of Jabal Salma, Saudi Arabia, Using Landsat Thematic Mapper Data

Philip A. Davis
U. S. Geological Survey, 2255 North Gemini Drive, Flagstaff, AZ 86001
Graydon L. Berlin
Department of Geography, Northern Arizona University, Flagstaff, AZ 86011

ABSTRACT: Landsat Thematic Mapper (TM) data were analyzed to determine how well they enable us to discriminate lithologic units, especially altered basalt deposits, within the complex geologic environment of Jabal Salma, Saudi Arabia. The analyses indicate that with the combination of bands 1, 4, and 5 or 7 we can unambiguously discriminate 84 percent of the mapped cinder cone and tuff deposits; these results are similar to those found for volcanic fields in the southwestern United States. Also, linear relations were found for iron concentrations and iron-oxidation ratios versus TM-band ratios of sample sites. Analyses of various TM color-composite images indicate that maximum discrimination of all rock types in this study area is provided by three color composites: bands 1, 4, and 5 or 7; the three principal components of bands 1, 4, and 5 or 7; and the band ratios 4/1, 5/4, and 7/5. These images enable discrimination among unaltered and altered basalt and rhyolite, gabbro, granite/syenite, monzogranite, sandstone, and complex metamorphic units.

INTRODUCTION

IN THIS PAPER we analyze Landsat Thematic Mapper (TM) data for the sparsely vegetated Jabal Salma region in Saudi Arabia, which contains many altered and unaltered basalt deposits. The region is more geologically complex than the three volcanic fields that we previously studied in the southwestern United States (Davis *et al.*, 1987). Igneous exposures in the Jabal Salma region range in composition from silicic to mafic, and metamorphic and sedimentary units are also present. The diversity in rock types in this region makes it a good test area to determine the usefulness of Landsat TM data for rock discrimination.

This study addresses the following questions: (1) Do Landsat TM bands 1, 4, and 5 (or 7) enable the high degree of discrimination between unaltered and altered basalt in the Jabla Salma region that is demonstrated for the southwestern United States? (2) Does a linear relation exist between iron content or iron-oxidation ratio and TM band 4/band 5 ratio for the olivine basalts in Jabal Salma similar to that found for the southwestern United States? (3) What Landsat TM data product or combination of products best enables discrimination between mapped geologic units, and how useful are various TM products for geologic mapping?

In a previous paper, we assessed the mineralogical and chemical factors that (1) control DN (digital number) values of the TM data and (2) make possible the discrimination of rock units within three volcanic fields in the southwestern United States (Davis *et al.*, 1987). These fields contain primarily altered and unaltered basalt and sedimentary rocks. The previous study showed that (1) most rock units can be discriminated on a color composite of TM bands 1, 4, and 5 (or 7); (2) discrimination among altered basalts, unaltered basalts, and sedimentary rocks is facilitated by different amounts of iron-oxide, carbonate, sulfate, and clay minerals in the rocks, which cause different amounts of absorption in the three TM reflective infrared bands (bands 4, 5, and 7); and (3) for olivine basalts, a linear correlation exists betwen Fe^{+2} concentration or Fe^{+2}/total-iron ratio and the values for the TM band 4/band 5 ratio. The present study builds on these results by examining Landsat TM data for the more geologically complex region of Jabal Salma.

DESCRIPTION OF THE STUDY AREA

The Jabal Salma region is located in north-central Saudi Arabia on the boundary between the Arabian Shield and the Arabian Shelf (Figure 1). Much of the study area is a plain of gentle relief, generally between 825 and 1000 m ASL, broken by isolated hills. The area also contains a striking feature, the rugged granite massif of Jabal Salma, where summit elevations approach 1300 m ASL (Figure 2). This region of Saudi Arabia lies in the "arid bioclimatic zone" that is characterized by a precipitation/potential evapotranspiration ratio of between 0.03 and 0.20 (UNESCO, 1977). Mean annual precipitation is 120 mm or

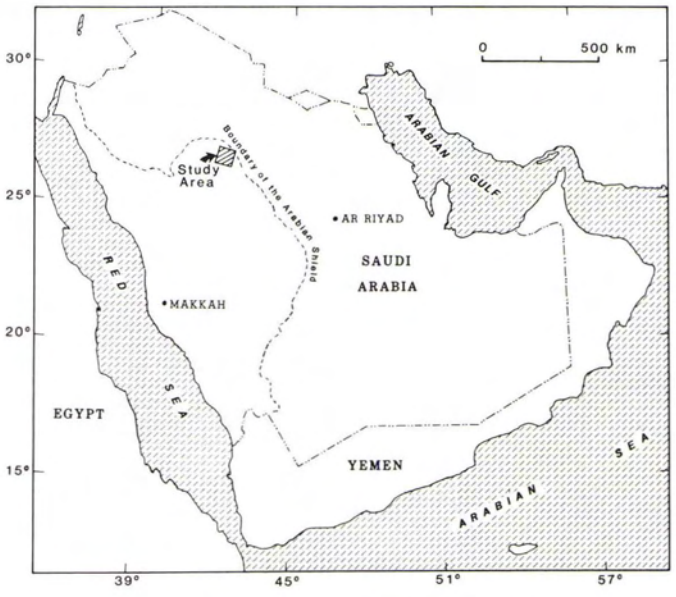

FIG. 1. Index map of Saudi Arabia showing location of Jabal Salma study area.

PHOTOGRAMMETRIC ENGINEERING AND REMOTE SENSING,
Vol. 55, No. 8, August 1989, pp. 1147-1160.

0099-1112/89/5508–1147$02.25/0

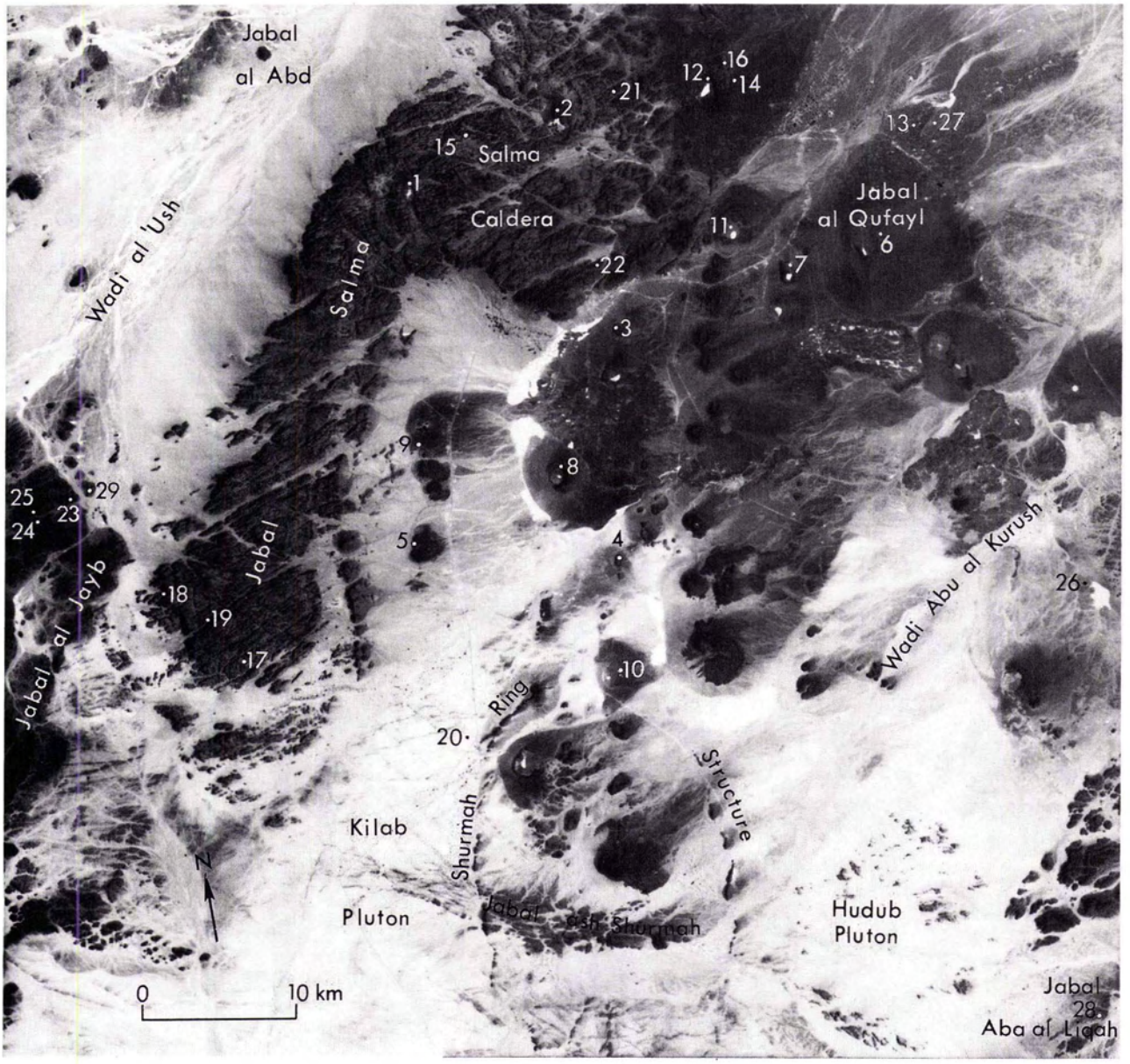

FIG. 2. Landsat-5 TM band 3 image of Jabal Salma study area. Numbered dots indicate sample sites.

less. Rainfall, although irregular and unpredictable, occurs mostly between November and March. Natural vegetation is restricted to scattered xerophytic shrubs and temporary grasses.

The study area has been mapped at a scale of 1:250,000, in part by the Bureau de Rescherches Géologiques et Miniéres (France) and in part by the U.S. Geological Survey. The geologic map shown in Plate 1 was generalized from portions of four published geologic maps (Williams *et al.*, 1986; Ekren *et al.*, 1987; Quick and Doebrich, 1987; Vaslet *et al.*, 1987).The study area is underlain largely by a Proterozoic assemblage of plutonic, metavolcanic, and metasedimentary rocks. The Proterozoic rocks are disconformably overlapped by a sandstone of Cambrian age and by a north-trending zone of basaltic cinder cones, tuff rings, and lava flows of Quaternary age that make up the Harrat Hutaymah volcanic field. Other Quaternary deposits, alluvium and poorly sorted colluvium, occur primarily in ephemeral wadi channels and sabkhahs and as a widespread veneer over pediment surfaces. In Table 1 we summarize the general outcrop color and mineral composition of the major rock units of the study area. In the following paragraphs we discuss the areal extent and general characteristics of the units. We discuss first the igneous and metamorphic units, from mafic to siliceous compositions, followed by the sedimentary units.

The Proterozoic basalt units within the study area have been metamorphosed to the greenschist facies; they include the Hibshi basalt, the Nuf basalt and andesite, the Banana basalt and andesite, and a tectonic melange (Table 1). These four units crop out in the southeast corner and along the west border of the study area (Plate 1). Gabbro exposures, which have been altered by serpentinization, are scattered throughout the western portion of the study area from Jabal al Abd in the north to the eastern border of the Kilab pluton in the south (Figure 2 and

TABLE 1. OUTCROP COLOR AND MINERAL CONSTITUENTS OF MAJOR ROCK UNITS IN JABAL SALMA REGION, SAUDI ARABIA[1].

Rock Group	Outcrop Color	Mineral Constituents[2]
Basalt flows and ash deposits	black to medium gray	Ol, Cp, Pl, Mt
Basalt cinder and tuff deposits	black to reddish brown	Ol, Cp, Pl, Mt, Hm
Metamorphosed basalts and andesites	black to dark greenish gray	Cp, Opx, Pl, Hb, Qz, Ch, Ep, Hm, Opq, Ca, Ap
Hibshi basalt		
Nuf basalt and andesite		
Banana basalt and andesite		
Tectonic melange	(orange red)	(Rhyodacite to dacite in matrix of highly altered basalt, andesite, and gabbro)
Gabbro	greenish black	Pl, Cp, Hb, Mt, Ac, serpentinized Ol
Diabase	dark gray	mostly Pl
Andesites and dacites	light to dark gray	Pl, Hb, Qz, Opq, Ch, Ca, Ep, Ap
Nuf andesite and dacite		
Hibshi andesite and dacite		(Interbedded with rhyolite tuff)
Turmus Formation (andesite)		(Interbedded with graywacke and conglomerate)
Rhyolites		
Hadn/Sufran rhyolite	red brown to black	Qz, Kf, Pl, Ep, Ch, Hb, Ca, Fl, Ga
Hibshi rhyolite	black to grayish red	Kf, Qz, Pl, Ep, Ch
Qarfa rhyolite	massive - chocolate layered - pinkish brown	Pl, Kf, Qz, Mt, Hm, Hb, Cp, Ap, Zr, Al
Alkali-felspar granites and syenites	light gray to pinkish brown	Kf, Pl, Qz, Bi, Ap, Ep, Ch, Zr, Al, Opq, Hm
Ni'ayy syenite		
Mubarriz syenite		
Unnamed syenite		
Salma granite		
Shurmah granite		
Hudub granite		
Iron-oxide granite	(orange brown)	
Monzogranites	light gray to pinkish gray	Kf, Mc, Pl, Qz, Bi, Hb, Opq
Abd monzogranite		
Ha'il monzogranite		
Kilab monzogranite	(white grus)	
Laban Complex	highly variable	Pl, Qz, Kf, Ch, Bi, Opq, Hb, Ep (Biotite-quartz diorite, tonalite, gabbro, granodiorite, monzogranite, and syenogranite)
Hibshi lithic sandstone	gray to dark green	(Mostly basalt and andesite fragments interbedded with shale, siltstone, and conghlomerate; fragments of dacite and diorite in matrix of silt and altered volcanic ash)
Hibshi conglomerate	gray to dark green	(Hibshi andesite and dacite clasts and mafic fragments of Laban Complex)
Nuf sedimentary "marble"	white to gray	Ca, Mt, Tr (Interlayered with basalt and andesite)
Rishi member of Saq sandstone	white to brown	Qz, Kf, Ms, Ca, Hm, Lm

[1]Extracted from Williams *et al.* (1986), Ekren *et al.* (1987), Quick and Doebrich (1987), and Vaslet *et al.* (1987).
[2]Mineral symbols: Ac (actinolite), Al (allanite), Ap (apatite), Bi (biotite), Ca (calcite), Ch (chlorite), Cp (clinopyroxene), Ep (epidote), Fl (fluorite), Ga (Garnet), Hm (hematite), Hb (hornblende), Kf (K feldspar), Lm (limonite), Mt (magnetite), Mc (microcline), Ms (muscovite), Ol (olivine), Opq (opaque minerals), Opx (orthopyroxene), Pl (plagioclase), Qz (quartz), Tr (tremolite), Zr (zircon).

Plate 1). A single exposure of diabase is located west of Jabal al Jayb.

The Quaternary basalt flows, ash deposits, and basaltic cinder cones and tuffs have virtually the same mineral compositions (Table 1), except that the cinder cones and tuffs have a significant amount of hematite resulting from alteration of their magnetite and iron-bearing silicate minerals. The hematite imparts a reddish-brown color to these deposits. The cinder cones and tuffs occur mostly at intersections of faults in the three major fault systems of the region (Plate 2): the Najd (WNW trend), Saqf (WSW trend), and Ha'il (NNE trend).

Three rock units have dominantly andesitic compositions--the Nuf andesite and dacite, the Hibshi andesite and dacite, and the Turmus Formation (Table 1). These units have been weakly metamorphosed. The Nuf andesite and dacite crops out on the west side of Jabal al Abd, the Hibshi andesite and dacite is exposed north of Jabal Aba al Liqah, and the Turmus Formation crops out east of Wadi Abu al Kurush (Figure 2 and Plate 1).

Four rhyolite units are contained within three formations: the Hadn/Sufran Formation (west of Jabal al Jayb), the Hibshi rhyolite (north of Jabal Aba al Liqah), and the Qarfa Formation (east side of Salma caldera). The Hadn/Sufran rhyolite is dominantly ash-flow tuffs and lava flows; the Hibshi rhyolite consists of massive flows. The Qarfa Formation consists of both a massive and a layered rhyolite ash-flow tuff; the layered tuff is locally coated by black desert varnish.

The alkali-feldspar granite/syenite rock group (Table 1) consists of seven units: the Ni-ayy and Mubarriz syenites and an unnamed syenite and the Salma, Shurmah, and Hudub granites and an iron-oxide granite. The Ni-ayy syenite is located mostly in the Salma caldera; the remainder of Jabal Salma is composed of the Salma granite (Figure 2 and Plate 1). The unnamed syenite crops out along the southern and eastern margins of Jabal

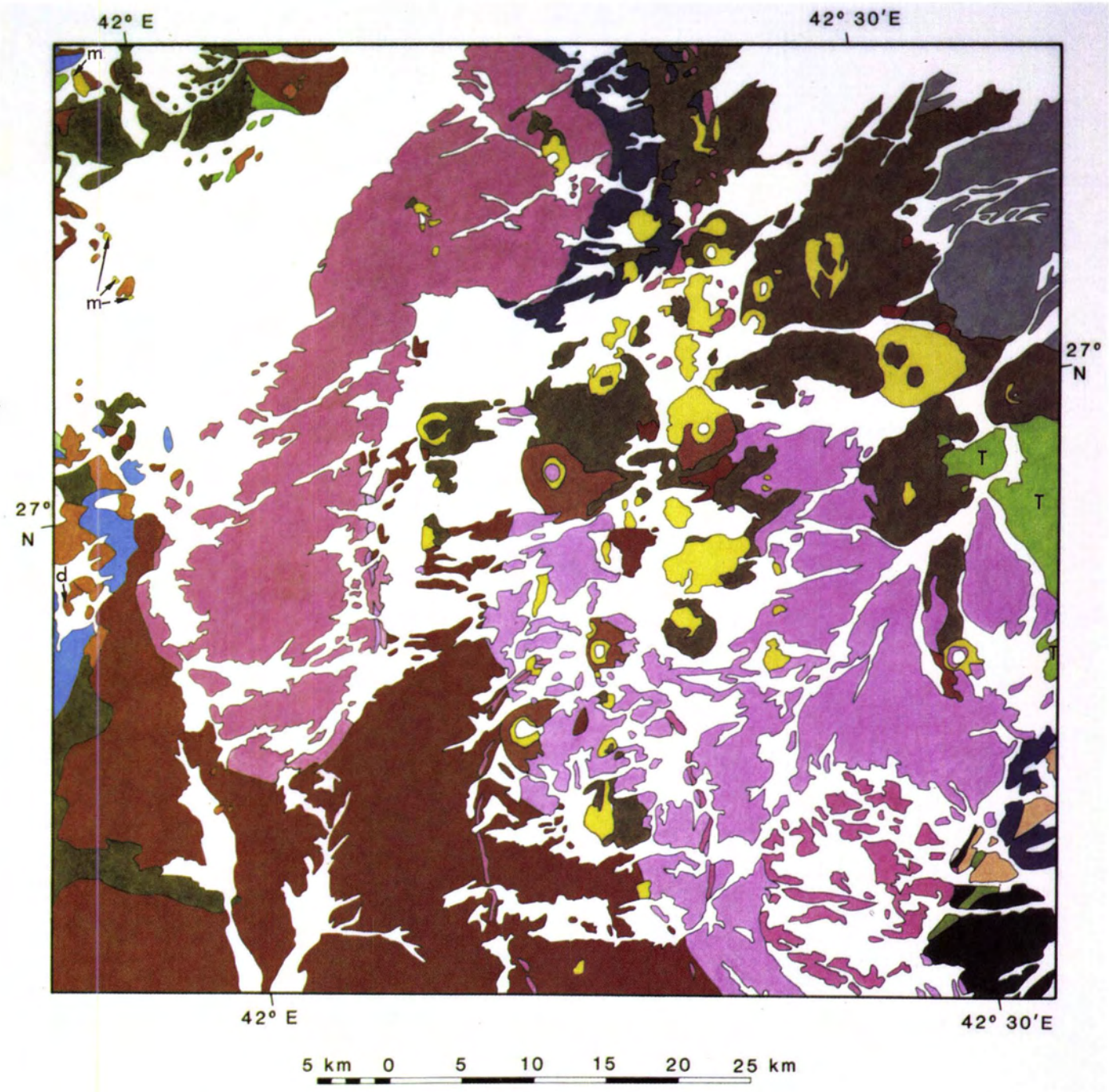

PLATE 1. Generalized geologic map of Jabal Salma area compiled from published 1:250,000-scale geologic maps (after Williams *et al.*, 1986; Ekren *et al.*, 1987; Quick and Doebrich, 1987; Vaslet *et al.*, 1987). Units in explanation not listed in stratigraphic order.

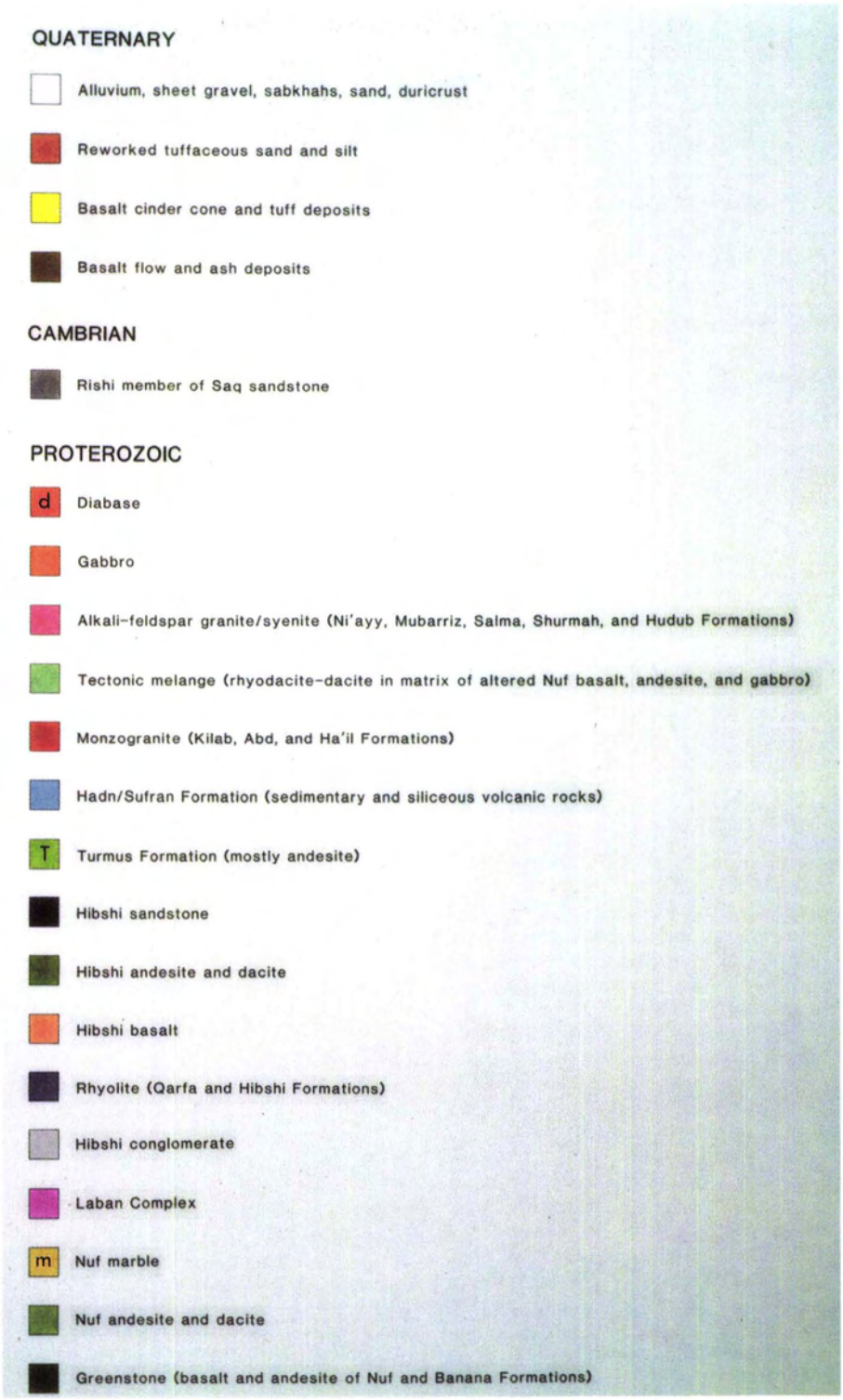
QUATERNARY
Alluvium, sheet gravel, sabkhahs, sand, duricrust
Reworked tuffaceous sand and silt
Basalt cinder cone and tuff deposits
Basalt flow and ash deposits
CAMBRIAN
Rishi member of Saq sandstone
PROTEROZOIC
d
Diabase
Gabbro
Alkali-feldspar granite/syenite (Ni'ayy, Mubarriz, Salma, Shurmah, and Hudub Formations)
Tectonic melange (rhyodacite-dacite in matrix of altered Nuf basalt, andesite, and gabbro)
Monzogranite (Kilab, Abd, and Ha'il Formations)
Hadn/Sufran Formation (sedimentary and siliceous volcanic rocks)
T
Turmus Formation (mostly andesite)
Hibshi sandstone
Hibshi andesite and dacite
Hibshi basalt
Rhyolite (Qarfa and Hibshi Formations)
Hibshi conglomerate
Laban Complex
m
Nuf marble
Nuf andesite and dacite
Greenstone (basalt and andesite of Nuf and Banana Formations)

PLATE 1. (Cont.)

Salma. The Mubarriz syenite and the iron-oxide granite form a ring of small, scattered exposures east of the rhyolite around Salma caldera (Figure 2 and Plate 1). The Shurmah granite is exposed in the Shurmah ring dike, and the Hudub granite is exposed in the Hudub pluton (Figure 2 and Plate 1).

The monzogranite rock group consists of the Abd, Ha'il, and Kilab units (Table 1). Of these, the Kilab is the most widely exposed in the study area, forming all monzogranite exposures in the south half (Plate 1). The Abd crops out in the northwest corner of the study area around Jabal al Abd; the Ha'il is represented by three small exposures east of Jabal al Qafayl (Figure 2 and Plate 1).

The Laban Complex is a heterogeneous rock unit that has been metamorphosed to the amphibolite facies; its mineralogy has been altered by chloritization and seritization. The Laban is the most widely exposed unit in the southeast quarter of the study area (Plate 1).

Four sedimentary rock units are present: the Hibshi lithic sandstone, the Hibshi conglomerate, the Nuf "marble," and the Rishi member of the Saq sandstone. The first three units are of Proterozoic age; the Saq sandstone is of Cambrian age. The two Hibshi units are exposed at Jabal Aba al Liqah (Figure 2 and Plate 1). The Nuf marble is represented by a few small, scattered exposures in the northwest corner of the study are (Figure 2 and Plate 1). The Rishi member crops out east of Jabal al Qafayl (Figure 2 and Plate 1).

LANDSAT DIGITAL DATA ANALYSIS AND RESULTS

The Jabal Salma region is contained within quadrant 4 of Landsat-5 TM scene 50170-07111, acquired 18 August 1984 (Figure 2) with a sun elevation angle of 58.2° and a sun azimuth angle of 109°.

The first step in most Landsat digital analyses is estimation of atmospheric scattering (commonly referred to as haze). Crippen (1987) reviewed previous methods for estimation of haze and proposed a new analysis called the regression intercept method (RIM), which requires at least two sites that have topography and spectral homogeneity but color differences. The intersection of the two regression lines for two such sites, if we use any two Landsat TM nonthermal bands, establishes the haze values for those two particular bands. Summit craters on some of the basalt cones in the study area are steep enough (near the angle of repose) to cast shadows. Because these dark areas may be merely shaded and may not represent true shadows, we performed Crippen's RIM analysis on several training sites that appeared to satisfy the basic requirements of such analysis. We found seven pairs of sites whose regression data satisfy additional criteria established by Crippen for determination of atmospheric scattering using the RIM. The haze values for each of the six nonthermal TM bands resulting from this RIM analysis, however, were higher than those observed within the steepest walled summit craters of the volcanic cones and along some of the steep walls of the dissected granite of Jabal Salma.

In Crippen's RIM analysis, the effects of some atmospheric parameters that contribute to the recorded signal in TM data are not considered. For example, skylight is assumed to have a negligible contribution to total illumination or to have spectral proportions similar to that of the direct illumination. Neither of these assumptions may be valid, especially the former. Thus, averages of the lower values within the shadowed areas were used as better estimates of atmospheric scattering. These haze values also correspond closely to haze values for a "clear" to "moderate" atmosphere as defined by Chavez (1988). The haze value for each nonthermal band was subtracted from the digital data for each respective TM band before beginning the digital analysis and processing described below.

Two types of digital analysis were performed on the TM data: (1) determination of band and band-ratio combinations that provide optimum discrimination for geologic mapping, and (2) determination of the TM reflectance characteristics of the major rock units, some of which were sampled in the field. The first analysis was performed before field sampling in order to select sample-collection sites. Two types of collection sites were chosen: sites that show inconsistency between the preliminary TM color products and published geologic maps and sites that appear spectrally homogeneous and representative of the major rock units. Care was exercised during field sampling to ensure that representative samples were obtained from each site (Figure 2 and Plate 2). Because resolution of the Landsat TM data is 30 m, each site was first examined by helicopter reconnaissance to evaluate surface homogeneity and to determine the necessary density of sampling. On the average, several samples were collected at each site over an area of about 2 km^2 (or four TM picture elements). Also, a priority was placed on sampling a sufficient number of altered and unaltered basalt exposures to determine the dependence of TM reflectance values on iron concentrations and iron-oxidation ratios. Unfortunately, there was not enough time to sample all 33 rock units shown on the 1:250,000-scale geologic maps, but a large proportion of these units differ only in age, location, texture, or minor mineralogy (e.g., six of the seven alkali-feldspar granites and syenites and the Qarfa layered and massive rhyolite units).

Statistical analysis methods were used on the six nonthermal TM bands to determine which combination of three bands and of three band ratios provide optimum information content, considering all combinations of three-band and three band-ratio data (Chavez *et al.*, 1982; Sheffield, 1985). Results obtained by the Sheffield method indicate that the best three-band combinations include TM bands 1, 3 (or 4), and 5 (or 7), as well as the combination of TM bands 1, 5, and 7. Visual analysis of color composites of the various three-band combinations corroborated the statistical results: of the 20 possible three-band combinations, the combination of TM bands 1, 4, and 5 (or 7) appears to provide the best discrimination among the various rock units in this study area (Plate 2). This same conclusion was reached in a study of three volcanic fields in the southwestern United States (Davis *et al.*, 1987). We also visually examined color composites of the 25 sets of three band-ratio combinations that were indicated as optimum by our statistical analyses. All of the band-ratio combinations that provide the best unit discrimination include band 5/band 4 and band 7/band 5 ratios and one of the following ratios: band 2/band 1, band 3/band 1, band 4/band 1, band 4/band 2, or band 3/band 2.

We performed a number of digital analyses beyond simple TM band and band-ratio compositing to examine the usefulness of additional TM products for geologic discrimination in the study area. These analyses included decorrelation stretching (Gillespie *et al.*, 1986) and principal component (PC) analysis, both of which we applied to the top-ranked TM band combinations mentioned previously. Visual inspection of all these color composites indicated that the best discrimination of the mapped rock units is provided by the band color-composite (BCC) image of TM bands 1, 4, and 5 (or 7) (Plate 2) and the principal-component color-composite (PCC) image of the first, second, and third components of the PC analysis on TM bands 1, 4, and 7 (Plate 3). Table 2 shows the percent of variance mapped to the three PCs and the loadings for TM bands 1, 4, and 7 that were used to produce the PCC image shown in Plate 3. These three PC images were also used in the decorrelation-stretch process, in which we linearly stretched the data in each of the PC images to fill, as much as possible, the 255 DN range while trying to

equalize the variances of the three PC images. An inverse PC transformation was then applied to these stretched data that resulted in three decorrelated-image files that were color composited.

The decorrelation-stretched composite of TM bands 1, 4, and 7 did provide more discrimination than the BCC of the simple linearly stretched TM bands 1, 4, and 7 within the bright saturated areas of the grus-covered monzogranite (Kilab pluton) and wihin the dark saturated areas of the basalt flows. It was difficult, however, to discriminate between some distinctly different geologic units (e.g., the red cinder cone deposits and the unvarnished granite on Jabal Salma) on the decorrelation-stretched images that were easily discriminated on the BCC of the simple linearly stretched TM bands 1, 4, and 7. Overall, the decorrelation-stretched versions of the TM band combinations provided no greater discrimination of rock units than did the PCC images. Thus, for this study area, the additional processing required for decorrelation stretching was not warranted.

Most of the 25 top-ranked band-ratio combinations provide no more discrimination than does the PCC image. The five top-ranked band-ratio combinations, which involve the TM band 5/band 4 ratio and the TM band 7/band 5 ratio, do enable discrimination of some rock units (gabbro in red and Saq sandstone in orange in Plate 4) that are not discriminated on either the PCC image (Plate 3) or the BCC image (Plate 2). The color assignments for the band ratios used in the band-ratio color-composite (BRC) image (Plate 4) were chosen to provide maximum discrimination of these two units (especially the small gabbro exposures). Alternative color assignments for the band ratios do provide better discrimination of the other rock units than that shown on Plate 4, but these alternate color assignments make discrimination of the gabbro and Saq sandstone very difficult because the human eye is less sensitive to shades of blue and green than to shades of red. The color images shown in Plates 2, 3, and 4 were used to select sample-collection sites for comparison of surface chemistry and mineralogy with TM reflectance values and for field verification of certain exposures.

DISCRIMINATION OF ALTERED BASALT DEPOSITS

In the BCC of TM band 1 (blue), TM band 4 (green), and TM band 5 or 7 (red), a one-percent linear contrast stretch was applied to both ends of each band's histogram. This composite provides easy discrimination between altered basalt deposits (red areas in Plate 2) and any other rock type, even unaltered basalts units. These altered basalts could not be discriminated on the natural-color (TM bands 1, 2, and 3) or standard false-color (TM bands 2, 3, and 4) images of this area that were produced using the method of Berlin and Chavez (1986). (These images are not shown because of reproduction cost.) This same conclusion was reached for the volcanic fields in the southwestern United States (Davis *et al.*, 1987). The BCC of TM bands 1, 4, and 7 (Plate 2) shows (as red anomalies) 33 of the 35 (94 percent) mapped basalt cinder cones and 14 of the 21 (67 percent) mapped basalt tuff deposits, or 84 percent of all basalt cinder cones and tuff deposits. This percentage compares well with the 89-percent detection level of basalt cinder cones on similar color composites of volcanic fields in the southwestern United States (Davis *et al.*, 1987). An additional eight red anomalies are shown on Plate 2 (arrows): five of these anomalies are within the mapped unaltered olivine basalt unit, two are within the mapped Laban Complex, and one is within the mapped Qarfa rhyolite unit. These cinder or tuff deposits were apparently missed by the regional mapping program at 1:250,000 scale. Thus, this simple TM BCC image provides a rapid and reliable method of detecting a high percentage of exposed deposits of altered (hematitic) basalt, even low-lying basalt squeeze-ups that may be missed by conventional field mapping.

Detection of altered basalt deposits using this TM BCC image also provides a remote-sensing technique for the detection of fault systems, because these deposits commonly occur at fault intersections (Plate 2). Without such a technique, traces of old fault systems are generally difficult to locate in younger volcanic fields unless the faults have been recently reactivated.

SAMPLE IRON CONTENT VERSUS LANDSAT TM BAND 4/BAND 5 RATIO

The locations of surface samples collected from the study area are shown on Figure 2 and Plate 2. Before removal of samples from a collection site, the average surface color of a site was determined by comparison with a soil or rock color chart (Munsell Color, 1954, Goddard *et al.*, 1948); color values of the collection sites are listed in Table 3. Procedures used in sample preparation and chemical analysis were described in Davis *et al.* (1987). The resulting concentrations of Fe_2O_3, FeO, and MnO are listed in Table 3. Average DN values of the six nonthermal TM bands for picture elements representing each sample site were obtained from the digital data. The DN values were corrected for atmospheric scattering by substraction of each band's haze DN value. These haze-corrected DNs were converted to band reflectance values using the method outlined in EOSAT (1986). The six nonthermal TM-band reflectance values for each sample collection site are listed in Table 3.

The statistical analysis by Davis *et al.* (1987) of iron concentration and TM-band values of altered and unaltered basalt within three volcanic fields in the southwestern United States indicates a linear relation between Fe^{+2} concentration or iron-oxidation ratios and TM band 4/band 5 DN ratio values. Similar least-squares analyses were performed on the altered and unaltered basalt sample sites of Jabal Salma using the TM-band reflectance values of the sample sites and the iron concentrations of the samples. As in our previous study, the strongest correlations were found between Fe^{+2}, Fe^{+2}/total Fe, and Fe_2O_3/total Fe and the TM band 4/band 5 ratio; all three regression lines from this analysis have an associated correlation coefficient of 0.880. Regression analyses using the TM band 1/band 5 ratio also resulted in high correlations (R^2 = 0.839 to 0.846). The single varnished basalt sample (1b) plots appreciably below the regression line, because the manganese-oxide minerals in the varnish, which are spectrally opaque, mask the true reflectance of the basalt. For that reason the varnished basalt sample was excluded in this analysis.

Our previous analysis of sample iron and sample-site TM data for the basalts in the southwestern United States used haze-corrected DN ratios of the sample sites, because equations for conversion to TM-band reflectance values were not yet available. Comparisons of these relations using different Landsat sensors (such as Landsat 4 versus Landsat 5) require normalization for the different detector gain and zero-offset settings, as well as for the different parameter values used in computer-processing the archive (raw) TM data (see EOSAT, 1986). Also, comparisons of Landsat data acquired during different seasons require normalization for the different solar-incidence angles. To compare the data of our previous study with those of the Jabal Salma region, we converted the haze-corrected DN values for the basalt sites in the southwestern United States to reflectance values, using tabulated values of the processing parameters for the 1982-1983 timeframe (EOSAT, 1986). Least-squares analyses of the TM-band reflectance ratios and Fe^{+2}, Fe^{+2}/total Fe, and Fe^{+3}/total Fe for the basalt sample sites and samples from the southwestern United States result in linear relations and associated correlation coefficients that are very similar to those found for the basalt samples from the Jabal Salma region. Results of least-squares

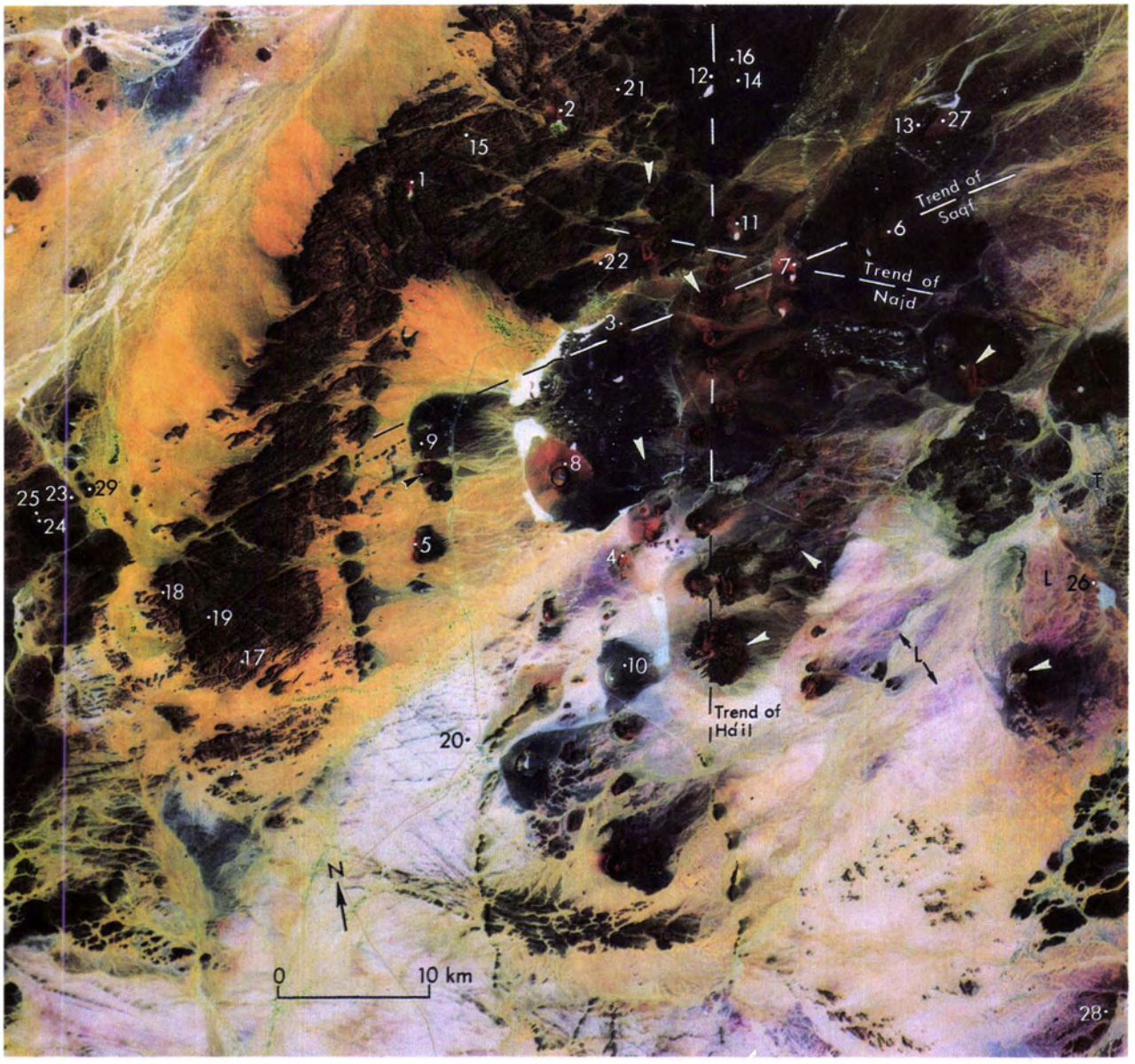

PLATE 2. TM-band color-composite (BCC) image of Jabal Salma area: Landsat TM band 1 displayed as blue, band 4 as green, and band 7 as red. Numbered dots indicate sample sites. Dashed lines show trends of three major fault systems. Arrows indicate cinder cone or tuff deposits detected by this false-color image that are not indicated on published geologic maps. Red areas are altered basalts. Letters indicate Turmus Formation (T) and Laban Complex (L).

analyses of the 37 combined basalt samples and sample sites from both of these studies are shown in Figure 3. Future field sampling of other volcanic fields will provide additional data that may further strengthen the statistical basis of these relations.

The relations between TM data and iron concentration and oxidation ratios are consistent with the locations of the major absorption bands of both Fe^{+2} and Fe^{+3}. The most common strongest absorption band for Fe^{+2} is between 1.0 μm and 1.1 μm (near TM band 4) from crystal field transitions of Fe^{+2} (Hunt and Salisbury, 1970). Fe^{+3} produces a strong absorption at about 0.4 μm (near TM band 1) from intervalence charge transfer between O^{-2} and Fe^{+3}, and weaker absorptions at about 0.45 μm, 0.49 μm (both within TM band 1), 0.7 μm (near TM band 3), and 0.87 μm (within TM band 4) from crystal field transitions (Hunt and Salisbury, 1970). Thus, the conversion of ferrous-iron-silicate minerals and magnetite to hematite results in less Fe^{+2} absorption in TM band 4 and more Fe^{+3} absorption in TM band 1, which causes an increase in slope between TM band 1 and TM band 5. This effect is demonstrated by comparisons of the TM-band reflectance data for the basalt flow and ash sample sites (Figure 4a) and for the cinder cone and tuff deposit sample sites (Figures 4b and 4c).

ROCK DISCRIMINATION USING LANDSAT TM DATA

The geologic map shown in Plate 1 is a generalized version of parts of four detailed published geologic maps that cover the Jabal Salma area. Although the original 33 mapped units were

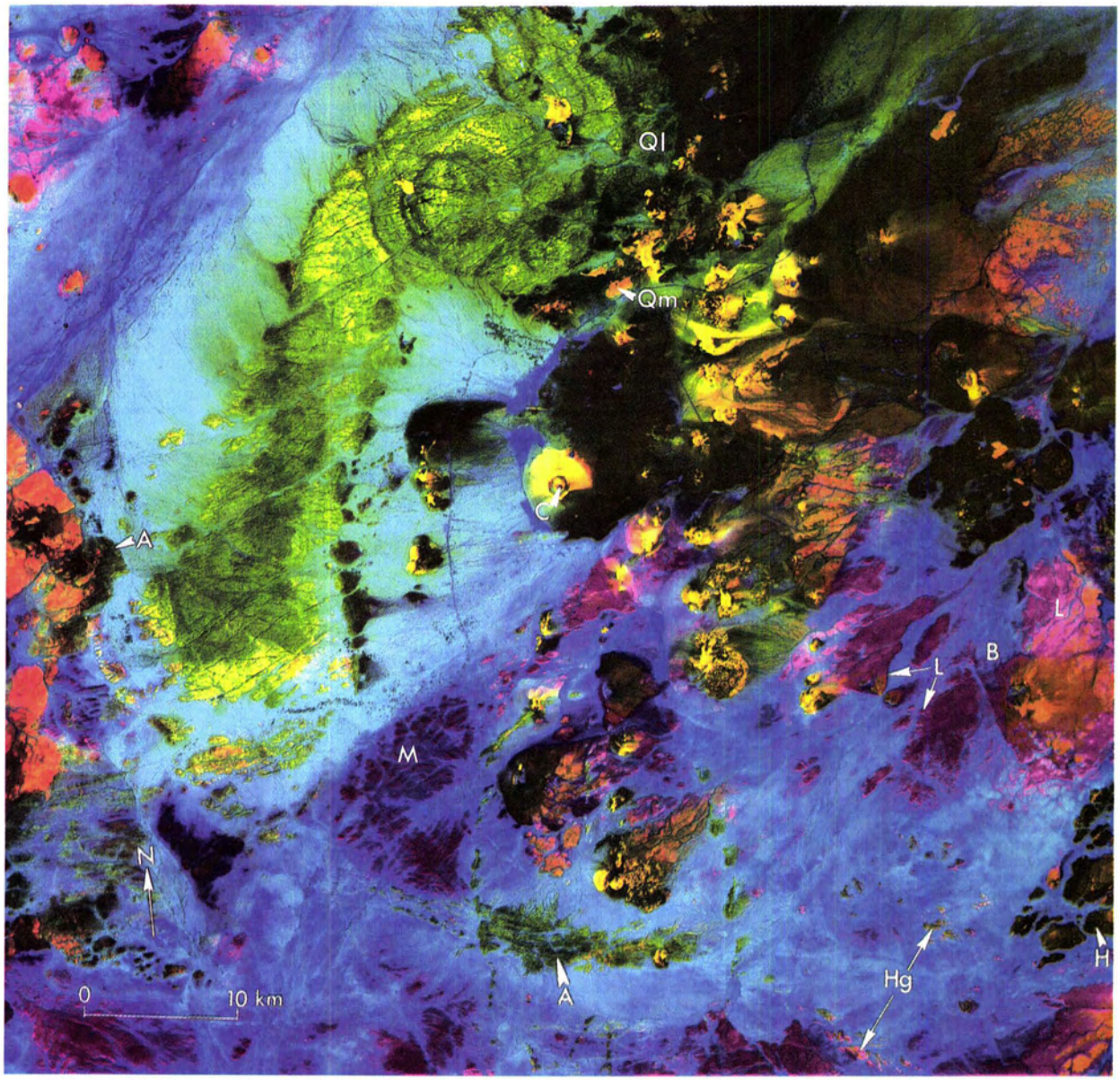

PLATE 3. Principal-component color-composite (PCC) image of Jabal Salma area resulting from principal-component analysis of TM bands 1, 4, and 7. Principal component 1 is displayed as blue, 2 as green, and 3 as red. Letters indicate representative areas of Hudub granite (Hg), Hibshi rhyolite (Hr), Qarfa layered rhyolite (Ql), Qarfa massive rhyolite (Qm), monzogranite (M), and Laban Complex (L), and probable areas of granite/syenite (A), basalt flow (B), and red cinder deposits (C) that were mapped as other rock units.

reduced to 21, unit distinction was retained where major mineralogy or rock type differs appreciably between mapped units. On the other hand, as discussed below, unit generalization was necessary to provide a fair test of rock discrimination using Landsat TM data. Certain obvious limitations occur in using reflectance energy bands for rock discrimination. For example, the data cannot be used to discriminate between geologic units mapped on the basis of location or age (e.g., the Salma, Shurmah, and Hudub granites) or subtle differences in feldspar composition (e.g., granites versus syenites, basalts versus andesites). Most minerals used to classify silicic rocks do not produce distinct spectral features (adsorptions) in visible and near-infrared (VNIR) wavelengths (Hunt and Salisbury, 1970). In addition, energy within VNIR wavelengths penetrates only about 20 to 30 μm below a rock's surface (Buckingham and Sommer, 1983). Thus, it is difficult to distinguish between rock units that are coated with iron- and manganese-oxide minerals (desert varnish), which are spectrally opaque, and between rock units that have similar weathering rinds (e.g., mafic volcanic rocks metamorphosed to greenschist facies). The comparisons that we make concern mostly discrimination of relatively distinct rock types (Plate 1). We have performed qualitative comparisons between the published geologic maps and the TM data rather than quantitative analyses (applying statistical analysis to a digitized

TABLE 2. PERCENT VARIANCE MAPPED TO PRINCIPAL COMPONENTS (PCS) AND LOADINGS FOR TM BANDS 1, 4, AND 7 FROM WHICH PC IMAGES OF JABAL SALMA, SAUDI ARABIA, WERE PRODUCED.

Principal Component	Percent Variance	Loadings		
		TM band 1	TM band 4	TM band 7
1	93.8	0.4616	0.5639	0.6848
2	5.2	−0.8311	0.0049	0.5562
3	1.0	0.3103	−0.8258	0.4709

geologic map and the TM data), because many of the geologic units are partly covered by surficial deposits (e.g., fluvial, alluvial, and eolian deposits) that would be difficult to exclude in the quantitative analysis.

After visual comparisons of TM color-composite images with the general geologic map, we found the following general conditions: (1) No single color-composite image provides discrimination of all the rock types shown on Plate 1; (2) of all the TM color-composite images, the best discrimination is provided by the PCC image (Plate 3), followed closely by the BCC image (Plate 2), both of which use TM bands 1, 4, and 7; and (3) the BRC images do not provide better discrimination than the PCC or BCC images for this study area. The BRC involving TM band ratios 5/4, 7/5, and 4/1 (Plate 4) does, however, discriminate two lithologic units (i.e., the gabbros and the Saq sandstone). Even though these two units make up only about 4 percent of the study area, discrimination of these units is important geologically because (1) the Saq sandstone indicates a change in geologic environment for this area in the Cambrian, and (2) altered gabbro exposures are commonly of economic importance. In the following paragraphs we discuss briefly the TM discrimination of various rock units in the study area.

The Quaternary basalt flow and ash deposits (dark brown on the PCC image, Plate 3; grayish-blue on the BCC image, Plate 2) are easily discriminated from the Quaternary cinder cone and tuff deposits (bright yellow on PCC, bright red on BCC). This discrimination is facilitated by the higher infrared reflectance values of the cinder cone and tuff deposits (due to hematite) compared to those of the basalt flows (Figures 4a and 4b). The color of the Turmus Formation (an andesite; area labeled "T" on Plate 2) on the PCC and BCC images is similar to that of the Quaternary basalt flows and ash deposits. This similarity is attributed to the close similarity of published reflectance spectra for andesites and basalts (Hunt *et al.*, 1973b).

The Hibshi rhyolite and the Qarfa layered rhyolite are best discriminated on the PCC image (Plate 3), where their color is olive green. The exposures of Qarfa massive rhyolite, on the other hand, have a yellow-orange color on the PCC image. Two reasons are proposed for the discrimination between the layered and massive rhyolites: (1) the layered rhyolite is generally more varnished than the massive rhyolite, which is indicated by the TM-band reflectance values (samples 21 and 22a, Figure 4e); and (2) secondary hematite is ubiquitous in the massive rhyolite, which results in elevated reflectance values for TM bands 5 and 7 (sample 22b, Figure 4e).

The alkali-feldspar granite/syenite units are distinguished from all other units by their light-green to yellowish-green color on the PCC image (Plate 3). Their TM-band reflectance values (samples 15 to 18, Figure 4d) are similar to published reflectance spectra of syenites (Hunt *et al.*, 1973b). Only the Hudub alkali-feldspar granite differs from the other units within the granite/syenite group by having both pink and light-green colors on the PCC image (Plate 3). The monzogranite units are easily discriminated from the granite/syenite units by their bluish-magenta color on the PCC image (e.g., area "M" on Plate 3). The monzogranites have higher overall TM-band reflectance values (sample 20, Figure 4d) than do the granites and syenites. In addition, the monzogranite exposures have very little relief (they are virtually flat lying) as opposed to the high relief of the alkali-feldspar granite/syenite exposures (Plates 1 and 2). Some of the areas mapped as monzogranite appear green on the PCC image and have high relief (e.g., areas labeled "A" on Plate 3), although green color and high relief are generally characteristic of the alkali-feldspar granite/syenite group.

The gabbro and diabase units have an orange color on the PCC image and a maroon color on the BCC image, but these colors are not unique to these two units. The BRC image (Plate 4), however, does uniquely discriminate most of the mapped gabbro exposures and the diabase (bright red color), but this image does not discriminate all of the mapped gabbro exposures. Most of the gabbro outcrops are weathered, and their olivine has been converted to serpentine. The presence of this hydroxyl-bearing mineral in gabbro usually results in absorption in the wavelength region of TM band 7 (Hunt and Salisbury, 1970; Hunt *et al.*, 1973a). The two gabbro sample sites in the study area do not show a marked depression in TM band 7 (samples 23 and 24, Figure 4f). TM-band reflectance values obtained from other mapped gabbro exposures (unsampled) do show a decrease in TM band 7 relative to TM band 5. Gabbro exposures that are not discriminated in the BRC image (Plate 4) are relatively unweathered, covered by alluvium, or smaller than the resolution of Landsat TM. The BRC image shows ten sites of probable gabbro exposures that are unmapped — one in the Nuf greenstone and one in the Nuf marble (both in the northwest corner of the study area) — and eight occurrences within the mapped Laban Complex within and around the Shurmah ring structure (Figure 2) in the southcentral part of the study area. The supposed gabbro anomaly within the Nuf marble on the BRC image may represent the marble itself, because carbonate in the metamorphosed limestone also causes an absorption in the wavelength region represented by TM-band 7 (Hunt and Salisbury, 1976b). The eight occurrences within the Laban Complex probably are exposures of the gabbro that occur in that composite unit.

The Laban Complex is represented by a bright-magenta color on the PCC image (e.g., areas labeled "L" on Plate 3). Its color is difficult to distinguish from that of the monzogranite in places, possibly because the monzogranite intrudes the Laban. The Laban consists of a composite of rock types ranging from mostly diorite to gabbro to monzogranite. Thus, the representation of this unit on the PCC image covers a range of colors from a bright magenta (similar, but not identical, to the blue magenta of the monzogranites) to orange (like the gabbros). The Laban is, however, easily discriminated from the monzogranite on the BCC image (Plate 2) by its purple color. The TM-band reflectance values of the sample site for the Laban (Figure 4f) are very similar to published reflectance spectra of hornblende diorites (Hunt *et al.*, 1973b). Two mapped exposures of Laban are not clearly indicated as such on either the PCC image (Plate 4) or the BCC image (Plate 2). One of these outcrops within a basalt flow (area "B" on Plate 3) is shown as mapped Laban on Plate 1; the other exposure is mapped within the summit crater of a cinder/tuff cone in the center of the study area ("C" on Plate 3). Both exposures were checked during our field sampling and proved to be a flow basalt and a combination of basalt cinders and sabkhah deposits, respectively, as suggested on both the PCC and BCC images.

The Rishi member of the Saq sandstone is not unambiguously discriminated on the BCC and PCC images. It is easily discriminated, however, on the BRC image (Plate 4), because its calcite and limonite cement cause absorption in the wavelength region

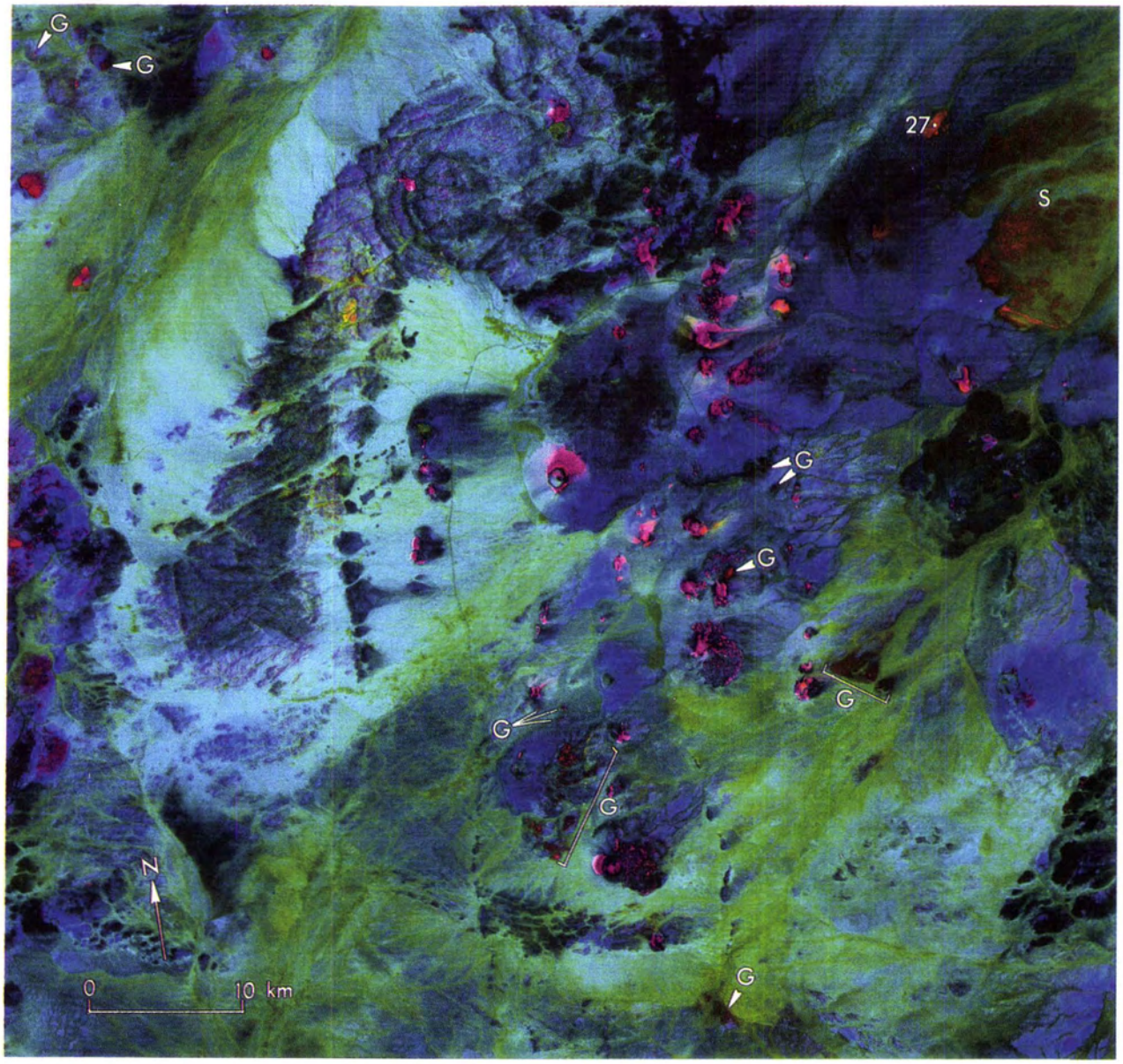

PLATE 4. TM band-ratio color-composite (BRC) image of Jabal Salma area: TM band 7/band 5 ratio displayed as blue, TM band 4/band 1 ratio displayed as green, and TM band 5/band 4 ratio displayed as red. Color assignments for TM band ratios accentuate the explosures of Saq sandstone (orange) and gabbro and diabase (bright red). Dot (27) indicates sample location of Saq sandstone. Lettered locations are probably areas of gabbro that were not mapped (G) and a representative area of Saq sandstone (S).

represented by TM band 7 (sample 27, Figure 4f; Hunt and Salisbury, 1971; Hunt *et al.*, 1971; Hunt and Salisbury, 1976a). The sample site for the Saq sandstone (Plate 4) was selected because of its sandstone color signature on the PCC, BCC, and BRC images within an area that is mapped as a basalt flow (Plate 1). Field and sample analysis proved this rock exposure to indeed be Saq sandstone (Table 3), as suggested by the TM images.

The remainder of the lithologic units within the study area consist mostly of mafic volcanic and sedimentary rocks that have been metamorphosed to the greenschist facies (some to the amphibolite facies). These units appear mostly as an orange color on the PCC image (Plate 3) and as a maroon color on the BCC image (Plate 2). The units include the Hibshi basalt, andesite and dacite, and conglomerate (in the southeast corner of the study area; Plate 1); the Nuf and Banana basalts and andesites (in the northwest and southwest corners, respectively); the Nuf andesites and dacites (in the northwest corner); and the Hadn/Sufran Formation (along west border of study area). The color of these units on the PCC and BCC images is similar to that of the gabbros, diabase, and Saq sandstone because the metavolcanic and metasedimentary rock units have secondary alteration minerals that include calcite, chlorite, and epidote (Table 1). These minerals characteristically show absorptions within the wavelength region represented by TM band 7 (Hunt and Salisbury, 1970, 1971; Hunt *et al.*, 1973a). Portions of these rock units are dark brown and dark green on the PCC image.

TABLE 3. ROCK TYPES SAMPLED, SURFACE COLOR, AVERAGE TM-BAND REFLECTANCE VALUES, AND IRON AND MANGANESE CONCENTRATIONS, OF SAMPLE-COLLECTION SITES IN JABAL SALMA REGION, SAUDI ARABIA

Sample Site- Description	Surface Color[1]	Landsat TM-band reflectance values[2] 1	2	3	4	5	7	Fe_2O_3 (wt %)	FeO (wt %)	MnO (wt %)
1a Basalt cinder	Pale reddish brown (10R 5/4)	0.052	0.084	0.134	0.189	0.409	0.435	11.60	0.24	0.19
1b Varn. basalt flow	Olive black (5Y 2/1)	0.051	0.074	0.113	0.139	0.162	0.175	3.28	2.95	0.94
2 Basalt cinder	Moderate reddish brown (10R 4/6)	0.055	0.084	0.126	0.165	0.343	0.372	8.65	2.98	0.19
3 Basalt cinder	Moderate reddish brown (10R 4/6)	0.059	0.089	0.130	0.171	0.346	0.351	10.85	0.65	0.17
4 Basalt cinder	Grayish red (10R 4/2)	0.055	0.079	0.121	0.159	0.354	0.378	10.35	0.17	0.15
5a Basalt cinder	Pale reddish brown (10R 5/4)	0.059	0.089	0.132	0.174	0.393	0.438	11.82	0.26	0.19
5b Basalt flow	Medium dark gray (N4)	0.056	0.082	0.122	0.157	0.201	0.204	7.35	3.60	0.19
6 Basalt tuff	Light brown (5YR 6/4)	0.064	0.094	0.132	0.168	0.283	0.270	8.44	1.14	0.14
7 Basalt tuff	Light brown (5YR 6/4)	0.066	0.101	0.154	0.204	0.397	0.421	7.56	1.26	0.14
8 Basalt tuff	Grayish red (10R 4/2)	0.066	0.096	0.140	0.183	0.397	0.401	12.28	0.75	0.18
9 Basalt tuff	Pale reddish brown (10R 5/4)	0.049	0.077	0.119	0.162	0.309	0.331	9.56	1.78	0.18
10 Basalt tuff	Medium dark gray (N3)	0.068	0.104	0.144	0.165	0.178	0.189	3.53	6.45	0.16
11a Basalt tuff	Grayish red (10R 4/2)	0.055	0.082	0.121	0.159	0.339	0.363	12.30	0.06	0.20
11b Basalt flow	Medium dark gray (N4)	0.058	0.084	0.119	0.142	0.150	0.152	10.96	2.73	0.74
12 Basalt flow	Brownish black (5YR 2/1)	0.051	0.072	0.101	0.130	0.159	0.157	4.39	6.33	0.22
13 Basalt flow	Medium gray (N4)	0.065	0.099	0.140	0.168	0.188	0.192	3.28	7.46	0.17
14 Basalt ash	Medium gray (N4)	0.052	0.074	0.097	0.115	0.111	0.111	3.64	6.89	0.17
15 Granite/syenite	Moderate reddish orange (10R 6/6)	0.061	0.092	0.142	0.201	0.290	0.320	1.10	0.21	0.04
16 Granite/syenite	Moderate reddish orange (10R 6/6)	0.062	0.096	0.142	0.177	0.199	0.209	2.95	1.70	0.13
17 Granite/syenite	Pale reddish brown (10R 5/4)	0.064	0.101	0.168	0.224	0.307	0.331	1.62	0.13	0.03
18a Granite/syenite	Dusky brown (5YR 2/2)	0.078	0.121	0.181	0.236	0.328	0.346	1.59	0.06	0.03
18b Varn. granite/syenite	Olive black (5Y 2/1)	0.064	0.101	0.159	0.204	0.247	0.262	1.30	0.20	0.14
19 Varn. granite/syenite	Olive black (5Y 2/1)	0.055	0.092	0.148	0.195	0.234	0.244	2.12	0.14	0.50
20 Monzogranite grus	Grayish orange pink (5YR 7/2)	0.142	0.213	0.297	0.366	0.417	0.427	2.12	1.07	0.07
21 Varn. rhyolite	Olive black (5Y 2/1)	0.052	0.084	0.134	0.174	0.206	0.204	2.71	0.02	1.47
22a Varn. rhyolite	Dusky brown (5YR 2/2)	0.058	0.092	0.144	0.174	0.173	0.175	3.77	1.00	0.26
22b Rhyolite	Pale reddish brown (10R 5/4)	0.064	0.099	0.144	0.177	0.251	0.279	2.99	1.53	0.10
23 Weathered gabbro	Light brown (5YR 5/6)	0.061	0.092	0.126	0.154	0.221	0.256	2.18	0.38	0.07
24 Varn. gabbro	Olive black (5Y 2/1)	0.056	0.084	0.121	0.142	0.143	0.146	2.00	0.57	0.07
25 Varn. Nuf greenstone	Dusky brown (5YR 2/2)	0.059	0.089	0.121	0.145	0.156	0.157	10.11	3.50	1.73
26 Laban Complex	Moderate brown (5YR 5/6)	0.087	0.128	0.175	0.213	0.294	0.314	4.30	5.16	0.22
27 Saq sandstone	Pale reddish brown (10R 5/4)	0.072	0.106	0.148	0.174	0.270	0.259	0.55	0.06	0.02
28 Hibshi sandstone	Brownish gray (5YR 4/1)	0.075	0.111	0.150	0.183	0.240	0.262	4.56	1.81	0.11
29 Varn. Hadn Formation	Olive black (5Y 2/1)	0.070	0.111	0.154	0.186	0.210	0.209	5.20	0.79	0.83

[1]Letter and number designations are those of Munsell Color Chart (Munsell Color, 1954) or Geol. Soc. Amer. Rock-Color Chart (Goddard *et al.*, 1948).

[2]Reflectance values calculated from haze-corrected TM-band DN using methods in EOSAT (1986).

These areas probably correspond to unaltered basalt and rhyolite exposures. Some of the units have a magenta color on the PCC image (similar to that of the Laban Complex). These units have either appreciable amounts of hornblende as a result of amphibolite-grade metamorphism (e.g., Nuf andesite and dacite) or contain fragments of the Laban Complex, which also has appreciable amounts of hornblende (e.g., Hibshi sandstone and conglomerate).

Overall, our examination of TM false-color composite images for the Jabal Salma area indicates the TM data can be used effectively to assist the field geologist in mapping complex geologic terrains. In this study area, the TM data permit unambiguous discrimination among altered and unaltered basalt, altered and unaltered rhyolite, gabbro, granite/syenite, monzogranite, a metadiorite complex, and a sandstone. TM data have certain limitations, however, for mapping purposes. First, they cannot be used to discriminate between rock types that differ only in the percentages of certain minerals that do not appreciably affect the wavelength regions defined by the TM bands. In this regard, it is very difficult to discriminate between granite and syenite rocks unless the exposures of the two rock types have weathered differently. In the Jabal Salma area, however, the TM data permit easy discrimination between the granite/syenite units and the monzogranite units. This discrimination may be facilitated by the preferential presence of hornblende in the monzogranites, but the marked differences in weathering characteristics between the granite/syenite and monzogranite probably play a large role in the discrimination. Second, different rock types that have been similarly weathered or that have undergone a similar grade of metamorphism may be difficult to discriminate with the TM data because the original mineralogical difference may be either obscured by a surface weathering rind or erased during metamorphic alteration.

CONCLUSIONS

We have shown that a color-composite image of Landsat TM bands 1, 4, and 5 or 7 enables discrimination of 84 percent of the mapped cinder cone and tuff deposits from all other rock units, including unaltered gray basalts. The discrimination is aided by the presence of hematite as a major mineral constituent in the cinder cone and tuff deposits. This conclusion is corroborated by the linear relations found between sample-site TM band 4/band 5 and band 1/band 5 ratios and sample ferrous iron concentration and iron-oxidation ratios. Similar TM discrimination and iron relations were found for three volcanic fields in the southwestern United States (Davis *et al.*, 1987). Thus, this simple TM-band color-composite image provides a rapid and reliable tool for detection of altered basalt deposits and the intersections of fault systems commonly indicated by the deposits' locations.

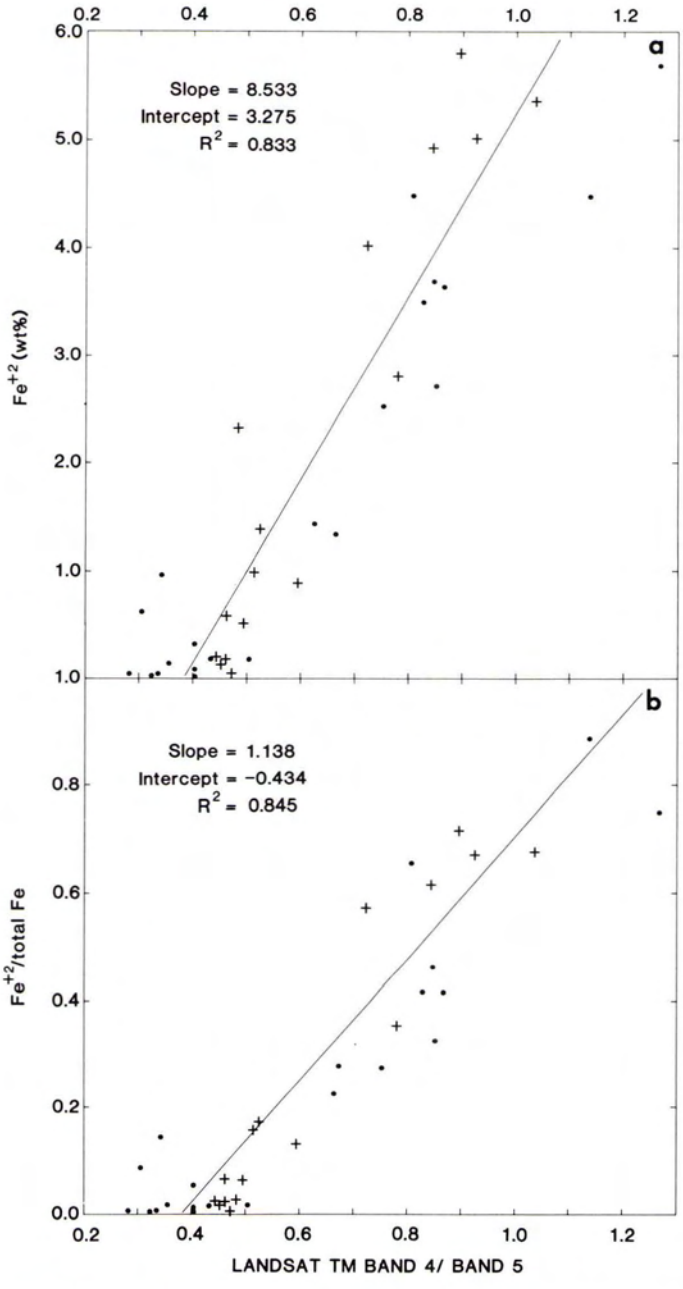

FIG. 3. Plot of sample-site TM band 4/band 5 ratio versus (a) Fe^{+2} concentration and (b) Fe^{+2}/total Fe ratio for olivine basalts from the Jabal Salma area. Crosses represent sample data for Jabal Salma area; dots represent sample data from Davis *et al.* (1987) for the southwestern United States. The regression lines represent least-squares fits to the data, which included consideration of the errors associated with both the ordinate and abcissa values for each data point (York, 1969).

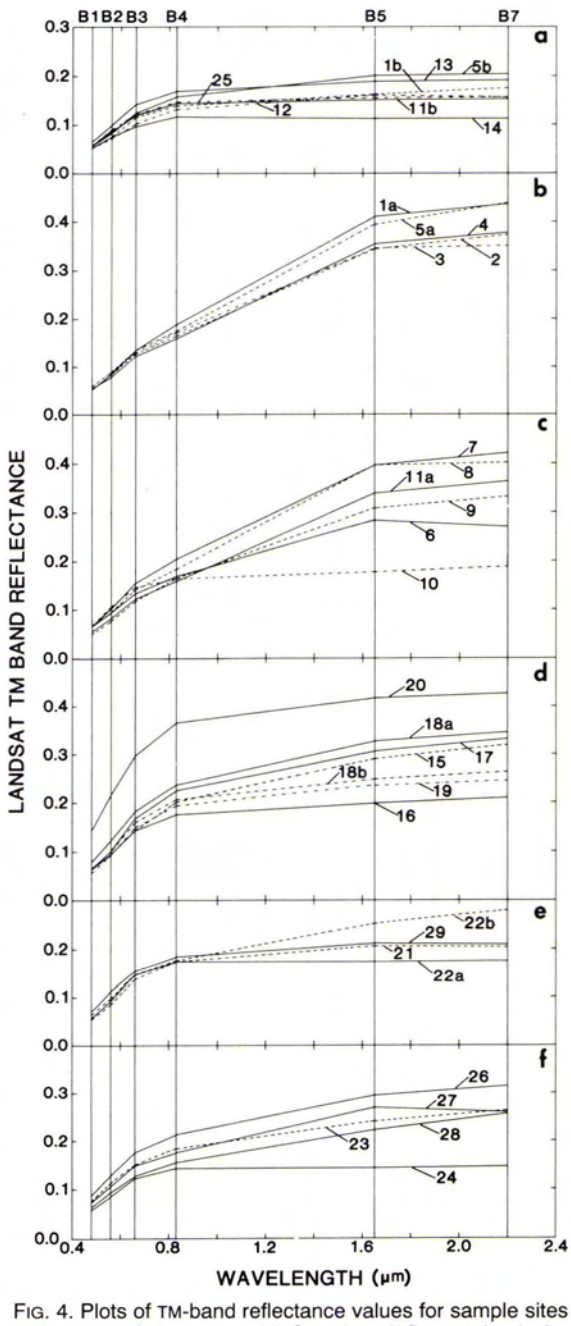

FIG. 4. Plots of TM-band reflectance values for sample sites in the Jabal Salma area. (a) Gray basalt flow and ash deposits and a greenstone [sample 25]. (b) Red basalt cinder deposits. (c) Basalt tuff deposits. (d) Granites/syenites and a monzogranite [sample 20]. (e) Rhyolites. (f) Gabbros [samples 23 and 24], sandstones [samples 27 and 28], and the Laban Complex [sample 26]. See Table 3 for identification of sample numbers not given above.

We have also shown that three TM color-composite images (bands 1, 4, and 5 or 7; the principal components of TM bands 1, 4, and 5 or 7; and the band ratios 4/1, 5/4, and 7/5) enable clear discrimination between most volcanic and sedimentary rock units in our particular test area. This discrimination is aided partly by differences in the mineral compositions of rock units and partly by differences in the weathering characteristics of the units. Even though the metamorphic rock units can be discriminated from the volcanic and sedimentary rock units on these images, discrimination between different mapped metamorphic rock units is difficult in this area because of the ubiquitous presence of similar alteration minerals that obscure differences in the original mineral composition of the rock units.

ACKNOWLEDGMENTS

The manuscript benefited from reviews by Pat Chavez, Alfred McEwen, and two anonymous reviewers. The authors also that

the technical support given by Ramon Sabala (drafting), Karl Zeller (photography), and Doris Weir (editing).

REFERENCES

Berlin, G. L., and P. S. Chavez, 1986. Quantitative procedure for producing color-calibrated Thematic Mapper natural-color images: *Fifth Thematic Conference—Remote Sensing for Exploration Geology*, Vol. 2, Environmental Research Institute of Michigan, pp. 638–648.

Buckingham, W. F., and S. E. Sommer, 1983. Mineralogical characterization of rock surfaces formed by hydrothermal alteration and weathering: Application to remote sensing: *Econ. Geol.*, Vol. 78, pp. 664–674.

Chavez, P. S., 1988. An improved dark-object subtraction technique for atmospheric scattering correction of multispectral data: *Remote Sensing of Environment*, Vol. 24, pp. 459–479.

Chavez, P. S., G. L. Berlin, and L. B. Sowers, 1982. Statistical method for selecting Landsat MSS ratios: *J. Applied Photographic Engineering*, Vol. 8, pp. 23–30.

Crippen, R. E., 1987. The regression intersection method of adjusting image data for band ratioing: *Intern. J. Remote Sensing*, Vol. 8, pp. 137–155.

Davis, P. A., G. L. Berlin, and P. S. Chavez, 1987. Discrimination of altered basaltic rocks in the southwestern United States by analysis of Landsat Thematic Mapper data: *Photogrammetric Engineering and Remote Sensing*, Vol. 53, pp. 45–55.

Ekren, E. B., D. Vaslet, A. Berthiaux, P. Le Strat, and J. Fourniquet, 1987. Geologic map of the Ha'il quadrangle, sheet 27E, Kingdom of Saudi Arabia (with text): *Saudi Arabian Deputy Ministry for Mineral Resources Geoscience Map GM-115C*, scale 1:250,000.

EOSAT, 1986. *Landsat Technical Notes*, No. 1, pp. 3–5.

Gillespie, A. R., A. B. Kahle, and R. E. Walker, 1986. Color enhancement of highly correlated images. I. Decorrelation and HSI contrast stretches: *Remote Sensing of Environment*, Vol. 20, pp. 209–235.

Goddard, E. N., P. D. Trask, R. K. De Ford, O. N. Rove, J. T. Singewald, Jr., and R. M. Overbeck, 1948. *Rock-color chart:* Washington, D.C., National Research Council, 8 p. (reprinted by Geol. Soc. Amer., 1951, 1963, 1970).

Hunt, G. R., and J. W. Salisbury, 1970. Visible and near-infrared spectra of rocks and minerals: I. Silicate minerals: *Modern Geology*, Vol. 1, pp. 283–300.

———, 1971. Visible and near-infrared spectra of rocks and minerals: II. Carbonates: *Modern Geology*, Vol. 2, pp. 23–30.

———, 1976a. Visible and near-infrared spectra of rocks and minerals: XI. Sedimentary rocks: *Modern Geology*, Vol. 5, pp. 211–217.

———, 1976b. Visible and near-infrared spectra of rocks and minerals: XII. Metamorphic rocks: *Modern Geology*, Vol. 5, pp. 219–228.

Hunt, G. R., J. W. Salisbury, and C. J. Lenhoff, 1971. Visible and near-infrared spectra of rocks and minerals. III. Oxides and hydroxides: *Modern Geology*, Vol. 2, pp. 195–205.

———, 1973a. Visible and near-infrared spectra of rocks and minerals: VI. Additional silicates: *Modern Geology*, Vol. 4, pp. 85–106.

———, 1973b. Visisble and near-infrared spectra of rocks and minerals: VIII. Intermediate igneous rocks: *Modern Geology*, Vol. 4, pp. 237–244.

Munsell Color, 1954 (revised 1975). *Munsell soil color charts:* Baltimore, Md., 20 p.

Quick, J. E., and J. L. Doebrich, 1987. Geologic map of the Wadi Ash Shu'bah quadrangle, sheet 26E, Kingdom of Saudi Arabia (with text): *Saudi Arabian Deputy Ministry for Mineral Resources Geoscience Map GM-108C*, scale 1:250,000.

Sheffield, C., 1985. Selecting band combinations from multispectral data: *Photogrammetric Engineering and Remote Sensing*, Vol. 51, pp. 681–687.

UNESCO, 1977. *Map of the Distribution of Arid Regions and Explanatory Note:* scale 1:25,000,000, United Nations, Paris, 54 p.

Vaslet, D., F. S. Kellogg, A. Berthiaux, P. Le Strat, and P. -L. Vincent, 1987. Geologic map of the Baq'a quadrangle, sheet 27F, Kingdom of Saudi Arabia (with text): *Saudi Arabian Deputy Ministry for Mineral Resources Geoscience Map GM-116C*, scale 1:250,000.

Williams, P. L., D. Vaslet, P. R. Johnson, A. Berthiaux, P. Le Strat, and J. Fourniquet, 1986. Geologic map of the Jabal Habashi quadrangle, sheet 26F, Kingdom of Saudi Arabia (with text): *Saudi Arabian Deputy Ministry for Mineral Resources Geoscience Map GM-98C*, scale 1:250,000.

York, D., 1969. Least squares fitting of a straight line with correlated errors: *Earth Planetary Science Letters*, Vol. 5, pp. 320–324.